Proceedings of the ASME 2020
International Design Engineering Technical Conferences
and Computers and Information in Engineering Conference
IDETC/CIE2020
August 17-19, 2020, Virtual, Online

DETC2020-22242

A NON-PRISMATIC BEAM ELEMENT FOR THE OPTIMIZATION OF FLEXURE MECHANISMS

Koen Dwarshuis[1], Ronald Aarts[1], Marcel Ellenbroek[1], Dannis Brouwer[1]

[1]University of Twente, Enschede, The Netherlands

ABSTRACT

Flexure joints are rapidly gaining ground in precision engineering because of their predictable behavior. However the range of motion of flexure joints is limited due to loss of support stiffness in deformed configurations. Most of the common flexure joints consist of prismatic leaf springs. This paper presents a simple non-prismatic beam formulation that can be used for the efficient modelling of non-prismatic leaf springs. The resulting stiffness and stress computed by the non-prismatic beam element are compared to the results of a finite element analysis. The paper shows that the support stiffness of two typical flexure joints can be increased up to a factor of 1.9 by using non-prismatic instead of prismatic leaf springs.

Keywords: Computational Mechanics, Compliant Mechanisms, Design Optimization

1. INTRODUCTION

Flexure joints are rapidly gaining ground in precision applications [1-4]. Flexure joints allow excellent predictable motion as they do not suffer from friction, backlash and have low hysteresis, in contrast to bearings. However their range of motion is limited due to loss of support stiffness under deformation. This limitation can potentially be reduced by using leaf springs that are non-prismatic instead of prismatic, i.e. leaf springs of which the width and the thickness vary over the length.

Literature has been published on the optimization of the shape of non-prismatic notch flexures [5, 6]. This research does not provide knowledge about flexure joints for large range of motion as notch flexures are typically used for a small range of motion. Tschiersky et all [7] showed that for a gravity compensation device with flexure springs the ratio between the elastic energy stored in the device and the weight could be increased by 94% by using a variable thickness of the leaf springs. To the best of the author's knowledge no other literature exists on the optimization of non-prismatic leaf springs for compliant devices undergoing large deformation.

A reason for not considering non-prismatic leaf springs is the lack of a fast and accurate modelling tool. Such a tool is essential as the shape of flexure joints can become relatively complex and design optimization is commonly used to optimize the designs of these joints [8, 9]. In order to perform these design optimizations, the flexure joint should be modelled in such way that deformation, stress and stiffness properties over the full range of motion can efficiently be computed. The past has shown that leaf springs can be modelled accurately with spatial beam elements using the software SPACAR [10]. The accuracy of the beam element in SPACAR is significantly improved by explicitly accounting for foreshortening [11]. However, this beam element does not allow an accurate modelling of non-prismatic flexures.

A simple modelling approach for the bending stiffness of non-prismatic beams is to use the Euler-Bernoulli or Timoshenko beam equations in which the variation of the stiffness coefficients is taken into account. In other words, the stiffness coefficients (e.g. EI) are written as functions of the axial coordinate. This approach is used for the two-dimensional static case [12-16] and to study vibration of beams [17, 18]. Rao and Gupta [19] used this approach for a three-dimensional rotating beam. Awtar and Sen [20] used this approach in the beam constraint model that takes nonlinear effects into account which arise from load equilibrium in deformed configurations. It should be noticed that this simple modelling approach results in a small error as shown by Boley [21]. Therefore more accurate modelling methods are proposed [22-24]. However these formulations are either only valid in two dimensions or the resulting equations are complex. For optimization purposes the simple approach is sufficiently accurate as the error introduced by this simplified approach is small for small variations of the cross section. However, this simplified approach is never

formulated in the generalized deformation formulation that is used in SPACAR.

In this paper a non-prismatic beam formulation is derived in the generalized deformation formulation and used to optimize the support stiffness of two different flexure joints. The beam formulation is presented in Section 2. The accuracy of the predicted stiffness is analyzed by a single leaf spring in Section 3. Section 4 shows optimization results for a parallel flexure guidance and Section 5 shows optimization results for a spherical flexure joint. The paper ends with the conclusions.

2. NON-PRISMATIC BEAM FORMULATION

This section derives a three-dimensional finite-strain non-prismatic beam formulation that accounts for foreshortening. Section 2.1 describes the relation between the forces and the displacements on both nodes of the beam. Section 2.2 expresses these relations in terms of deformation modes to obtain a stiffness matrix. Section 2.3 presents an expression to account for the foreshortening effect. Section 2.4 gives notes about the implementation of the element.

2.1 Relation between nodal forces and nodal displacements

In this section the relations between forces and displacements are derived by integrating the elasticity coefficients over the length of the beam. The resulting integrals are denoted by G_i. The integrals will not be evaluated analytically, although these integrals can be evaluated for many standard variations in the cross section [14, 15, 17]. Evaluating the integrals numerically allows for more freedom in the variation of the cross section and only little computation time is required for this numerical integration.

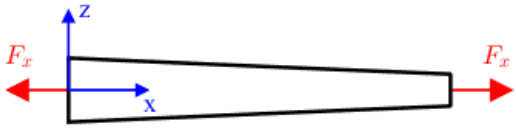

FIGURE 1: AXIAL DEFORMATION

Axial deformation. Figure 1 shows a beam on which axial force is applied. The resulting axial displacement can be computed from:

$$u(\xi) = u_0 + F_x L_0 \int_0^{\xi} \frac{1}{EA(s)} ds, \tag{1}$$

where ξ is the natural x-coordinate of the undeformed configuration ($\xi \equiv x/L_0$), u_0 is the displacement of the left node, F_x is the axial force, L_0 is the undeformed length of the beam, E is the elasticity and A is the cross sectional area which depends on the x-coordinate. s is the integration variable. The integral-term will be denoted by $G_1(\xi)$:

$$G_1(\xi) \equiv \int_0^{\xi} \frac{1}{EA(s)} ds, \tag{2}$$

The relation between the axial displacement of the left and right node and the forces on the nodes can therefore be expressed as:

$$u_L - u_0 = F_x L_0 G_1(1), \tag{3}$$

where u_L is the displacement of the right node. Henceforth we will omit the argument of an integral G_i if it is evaluated at 1, so $G_1 \equiv G_1(1)$.

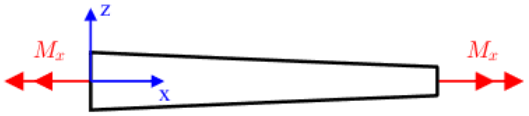

FIGURE 2: TORSION

Torsion. Torsion is shown in Fig. 2 and can be computed by:

$$\phi_x(\xi) = \phi_{x0} + M_x L_0 \int_0^{\xi} \frac{1}{GI_t(s)} ds, \tag{4}$$

where ϕ_{x0} is the rotation around the local x-axis of the left node, M_x is the applied moment, G is the shear modulus and I_t is the polar moment of inertia. By introducing:

$$G_2(\xi) \equiv \int_0^{\xi} \frac{1}{GI_t(s)} ds, \tag{5}$$

we can write:

$$\phi_{xL} - \phi_{x0} = M_x L_0 G_2, \tag{6}$$

where ϕ_{xL} is the rotation of the right node.

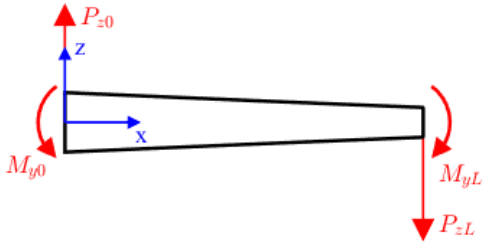

FIGURE 3: BENDING IN XZ-PLANE

Bending in xz-plane. Figure 3 shows the bending in the xz-plane. The internal moment around the y-axis is:

$$M_y(\xi) = M_{y0} - P_{z0} L_0 \xi. \tag{7}$$

The rotation around the y-axis, ϕ_y in the beam is:

$$\phi_y(\xi) = \phi_{y0} + \int_0^{\xi} \frac{M_y(s)}{EI_y(s)} ds, \tag{8}$$

where I_y is the second moment of area around the y-axis. By substituting eq. (7), we obtain:

$$\phi_y(\xi) = \phi_{y0} + M_{y0}L_0G_{31}(\xi) - P_{z0}L_0^2G_{32}(\xi), \quad (9)$$

where:

$$G_{31}(\xi) \equiv \int_0^\xi \frac{1}{EI_y(s)}ds\,, G_{32}(\xi) \equiv \int_0^\xi \frac{s}{EI_y(s)}ds. \quad (10)$$

The displacement in the z-direction can be obtained by integrating the y-rotation over the x-coordinate and including the deformation due to shear:

$$w(\xi) = w_0 - L_0\int_0^\xi \phi_y(s)ds - P_{z0}\int_0^\xi \frac{1}{GA(s)k_y(s)}ds, \quad (11)$$

where k_y is the shear correction coefficient according to Cowper [25] that account for the non-uniform distribution of the shear stress over the cross-section. By defining:

$$G_{33}(\xi) \equiv \int_0^\xi G_{31}(s)ds, \qquad G_{34}(\xi) \equiv \int_0^\xi G_{32}(s)ds - \frac{1}{L_0^2}\int_0^\xi \frac{1}{GA(s)k_y(s)}ds, \quad (12)$$

we can express the displacement in the z-direction like:

$$w(\xi) = w_0 - \phi_{y0}L_0\xi - M_{y0}L_0^2G_{33}(\xi) + P_{z0}L_0^3G_{34}(\xi). \quad (13)$$

Eqs. (9) and (13) can be evaluated at the right node of the beam, i.e. at $\xi = 1$, and combined to:

$$\begin{Bmatrix} \phi_{yL} - \phi_{y0} \\ w_L - w_0 + \phi_{y0}L_0 \end{Bmatrix} = \begin{bmatrix} L_0G_{31} & -L_0^2G_{32} \\ -L_0^2G_{33} & L_0^3G_{34} \end{bmatrix} \begin{Bmatrix} M_{y0} \\ P_{z0} \end{Bmatrix}. \quad (14)$$

This is a relation between the nodal displacements and nodal forces in the xz-plane in terms of 4 integrals. However there exist a relation between three of these integrals which means that only three integrals have to be evaluated to obtain the relation between nodal forces and displacements. To show this relation, the rule of partial integration can be used, which implies that for two arbitrary functions $f(\xi)$ and $g(\xi)$:

$$\int_0^1 f(\xi)g'(\xi)d\xi = [f(\xi)g(\xi)]_0^1 - \int_0^1 f'(\xi)g(\xi)d\xi. \quad (15)$$

By substituting $f(\xi) = \xi$ and $g(\xi) = \int_0^\xi 1/EI_y(s)\,ds$:

$$\int_0^1 \xi\frac{1}{EI_y(\xi)}d\xi = \left[\xi\int_0^\xi \frac{1}{EI_y(s)}ds\right]_0^1 - \int_0^1 1\int_0^\xi \frac{1}{EI_y(s)}ds\,d\xi, \quad (16)$$

which is equivalent to $G_{32} = G_{31} - G_{33}$. This relation is used to substitute G_{33} in eq. (14):

$$\begin{Bmatrix} \phi_{yL} - \phi_{y0} \\ w_L - w_0 + \phi_{y0}L_0 \end{Bmatrix} = \begin{bmatrix} L_0G_{31} & -L_0^2G_{32} \\ -L_0^2(G_{31} - G_{32}) & L_0^3G_{34} \end{bmatrix} \begin{Bmatrix} M_{y0} \\ P_{z0} \end{Bmatrix}. \quad (17)$$

This is a relation between the nodal displacements and nodal forces in the xz-plane in terms of 3 integrals.

Bending in the xy-plane. The relation between forces and displacements in the xy-plane can obtained similar to the derivation for the xz-plane, resulting in:

$$\begin{Bmatrix} \phi_{zL} - \phi_{z0} \\ v_L - v_0 - \phi_{z0}\,L_0 \end{Bmatrix} = \begin{bmatrix} L_0G_{51} & L_0^2G_{52} \\ L_0^2(G_{51} - G_{52}) & L_0^3G_{54} \end{bmatrix} \begin{Bmatrix} M_{z0} \\ P_{y0} \end{Bmatrix}, \quad (18)$$

where G_{51} till G_{54} are similar to G_{31} till G_{34}, except from the fact that I_y and k_y are replaced by I_z and k_z respectively.

This section showed the relation between nodal forces and nodal displacements in terms of 10 integrals that only depend on the distribution of the elasticity coefficients over the length of the beam-element.

2.2 Stiffness in terms of deformation modes

The previous section showed a relation between nodal forces and displacement for a specific choice of the position of the local frame of the element. The relations are therefore not directly applicable in a three-dimensional multibody analysis with multiple elements. This section will define deformation modes and use the relations from the previous subsection to derive the stiffness matrix in terms of these deformation modes. The chosen deformation modes are similar to the deformation modes defined by Jonker and Meijaard [11]. They defined relations between the deformation modes and three-dimensional absolute nodal coordinates such that the stiffness matrix of these deformation modes can be used in a 3D multibody analysis, as explained in Section 2.4.

The generalized coordinates of the deformation modes are referred to as strains and denoted by ε_i. These strains are related to the nodal displacements that are defined in Section 2.1. This relations are called boundary conditions and listed in Fig. 4.

(a) Axial deformation

B.C.: $u_0 = 0,$
$u_L = \varepsilon_1.$

Stress: $\sigma_1 = F_x.$

$$S_{11} = \frac{1}{L_0 G_1}$$

(b) Torsion

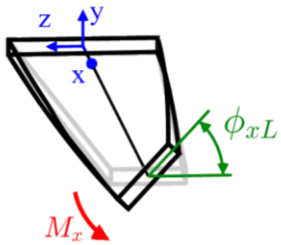

B.C.: $\phi_{x0} = 0,$
$\phi_{xL} = \varepsilon_2 / L_0.$

Stress: $\sigma_2 = M_x / L_0.$

$$S_{22} = \frac{1}{L_0^3 G_2}$$

(c) Bending in the xz-plane

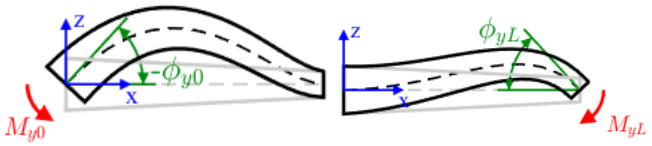

B.C.: $w_0 = 0,$ $w_L = 0,$
$\phi_{y0} = -\varepsilon_3 / L_0,$ $\phi_{zL} = \varepsilon_4 / L_0.$

Stress: $\sigma_3 = M_{y0} / L_0,$ $\sigma_4 = M_{yL} / L_0.$

$$\begin{bmatrix} S_{33} & S_{34} \\ S_{43} & S_{44} \end{bmatrix} = \frac{1}{L_0^3 D_3} \begin{bmatrix} -G_{32} + G_{34} & G_{34} \\ G_{34} & -G_{31} + G_{32} + G_{34} \end{bmatrix}$$

where $D_3 = G_{31} G_{34} - G_{32} G_{31} + G_{32}^2.$

(d) Bending in the xy-plane

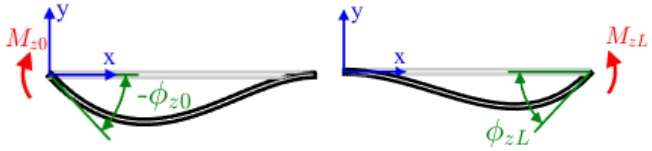

B.C.: $v_0 = 0,$ $w_L = 0,$
$\phi_{z0} = -\varepsilon_5 / L_0,$ $\phi_{zL} = \varepsilon_6 / L_0.$

Stress: $\sigma_5 = M_{z0} / L_0,$ $\sigma_6 = M_{zL} / L_0.$

$$\begin{bmatrix} S_{55} & S_{56} \\ S_{65} & S_{66} \end{bmatrix} = \frac{1}{L_0^3 D_5} \begin{bmatrix} -G_{52} + G_{54} & G_{54} \\ G_{54} & -G_{51} + G_{52} + G_{54} \end{bmatrix}$$

where $D_5 = G_{51} G_{54} - G_{52} G_{51} + G_{52}^2.$

FIGURE 4: DEFORMATION MODES WITH CORRESPONDING BOUNDARY CONDITIONS, STRESS AND STIFFNESS RELATIONS.

The generalized forces of the modes are called stress resultants, and are denoted by σ_i. According to the principle of virtual work, the element is in state of equilibrium if:

$$\delta \boldsymbol{u}^T \boldsymbol{F} = \delta \boldsymbol{\varepsilon}^T \boldsymbol{\sigma}, \tag{19}$$

where $\boldsymbol{u}$ is the vector with the 12 nodal displacements (the 3 translations, u, v and w and the 3 rotations ϕ_x, ϕ_y and ϕ_z for both nodes of the element) and $\boldsymbol{F}$ is the vector with forces in the same directions (the 3 forces F_x, F_y and F_z and 3 moments M_x, M_y and M_z for both nodes of the element).
Because the boundary conditions relate the nodal displacements, $\boldsymbol{u}$, to the strains, $\boldsymbol{\varepsilon}$, eq. (19) can be used to define relations between the stress resultants and nodal forces. These relations are given in Fig. 4 and referred to as stress relations.

The stiffness relation between the strains and stress resultants can be expressed by a stiffness matrix like:

$$\begin{Bmatrix} \varepsilon_1 \\ \varepsilon_2 \\ \varepsilon_3 \\ \varepsilon_4 \\ \varepsilon_5 \\ \varepsilon_6 \end{Bmatrix} = \begin{bmatrix} S_{11} & & & & & \\ & S_{22} & & & & \\ & & S_{33} & S_{34} & & \\ & & S_{43} & S_{44} & & \\ & & & & S_{55} & S_{56} \\ & & & & S_{65} & S_{66} \end{bmatrix} \begin{Bmatrix} \sigma_1 \\ \sigma_2 \\ \sigma_3 \\ \sigma_4 \\ \sigma_5 \\ \sigma_6 \end{Bmatrix} \tag{20}$$

The coefficients S_{ij} can be obtained by substituting the boundary conditions and stress relations in the equations of Section 2.1 as explained below. For the axial deformation, S_{11} can be obtained by substituting the boundary conditions and stress relations in eq. (3). The stiffness coefficient for torsion, S_{22}, can be obtained using eq. (6). For bending in the xz-plane, the boundary conditions and stress relations can be substituted in eq. (17), and the result can be rewritten to:

$$\begin{Bmatrix} \varepsilon_5 \\ \varepsilon_6 \end{Bmatrix} = L_0^3 \begin{bmatrix} G_{31} - G_{32} - G_{34} & G_{34} \\ G_{34} & G_{32} - G_{34} \end{bmatrix} \begin{Bmatrix} \sigma_5 \\ \sigma_6 \end{Bmatrix} \tag{21}$$

Inverting this matrix results in the stiffness coefficients that are given in Fig. 4 (c). The stiffness coefficients for the xy-plane can be obtained similarly.

2.3 Second order expression for axial deformation

The axial elongation is influenced by bending, this effect is called foreshortening. A better approximation for the axial deformation as defined in the first strain is therefore [11, 26]:

$$\hat{\varepsilon}_1 = \int_0^L \frac{du}{dx} + \frac{1}{2}\left(\frac{dv}{dx}\right)^2 + \frac{1}{2}\left(\frac{dw}{dx}\right)^2 dx, \tag{22}$$

The evaluation of the first term in this integral equals the earlier introduced strain ε_1. The lateral displacements v and w can be expressed in terms of the strains ε_3 till ε_6 as explained below. To obtain w, the nodal forces P_{y0} and nodal force moment M_{z0} can be expressed in terms of the nodal displacements by eq. (17) and

then substituted in eq. (13). This gives an expression for w in terms of the nodal displacements. After substituting the boundary conditions from Fig. 4 (c), the displacement w is expressed in terms of ε_3 and ε_4:

$$w(\xi) = N_3(\xi)\varepsilon_3 + N_4(\xi)\varepsilon_4, \tag{23}$$

where N_3 and N_4 are the mode shapes corresponding to the third and fourth strain respectively:

$$N_3(\xi) = \xi + \frac{(G_{32} - G_{34})G_{33}(\xi) - G_{32}G_{34}(\xi)}{D_3}, \tag{24}$$

and:

$$N_4(\xi) = -\frac{G_{34}G_{33}(\xi) - G_{33}G_{34}(\xi)}{D_3}, \tag{25}$$

In order to obtain the derivative dw/dx, the derivatives of the modes shapes $N_3(\xi)$ and $N_4(\xi)$ should be derived, which can be obtained using:

$$\frac{dG_{33}}{d\xi} = G_{31}(\xi), \qquad \frac{dG_{34}}{d\xi} = G_{32}(\xi) - \frac{1}{GA(\xi)k}. \tag{26}$$

Similar to the displacement w, the displacement v can be expressed in terms of $N_5(\xi)$, $N_6(\xi)$, ε_5 and ε_6. We can now define $\hat{\varepsilon}_1$ in terms of the other strains:

$$\hat{\varepsilon}_1 = \varepsilon_1 + \frac{1}{2L_0}[H_{33}\varepsilon_3^2 + 2H_{34}\varepsilon_3\varepsilon_4 + H_{44}\varepsilon_4^2 + H_{55}\varepsilon_5^2 + 2H_{56}\varepsilon_5\varepsilon_6 + H_{66}\varepsilon_6^2], \tag{27}$$

where: :

$$H_{ij} \equiv \int_0^1 \frac{dN_i}{d\xi}\frac{dN_j}{d\xi}d\xi. \tag{28}$$

The terms H_{ij} are 6 integrals that depend on the variation of the stiffness over the length of the beam. By eq. (27) the second order axial strain is expressed in terms of the other strains, which means that it can be computed easily.

2.4 Implementation

The non-prismatic beam element is implemented in SPACAR [10] to validate the 3D static analyses. SPACAR describes the configuration of a mechanism based on the strains (deformation coordinates) and the three-dimensional absolute nodal coordinates. The implementation of an new element for static analyses requires two kind of relations. In the first place the stiffness relations in terms of the deformation modes as given in eq. (20). Secondly kinematic relations between the strains and the nodal coordinates $\boldsymbol{x}$:

$$\boldsymbol{\varepsilon} = \boldsymbol{\mathcal{D}}(\boldsymbol{x}), \tag{29}$$

The deformation modes of the non-prismatic beam element are chosen such that this relation is exactly the same as the linear relation defined in equations 5-7 of reference [11]. Therefore the linear relations in equations 5-14 of reference [11] can be used for the implementation. These linear relations are modified based on eq. (27) to implement the nonlinear foreshortening effect that is derived in Section 2.3.

3. ANALYSIS OF A LEAF SPRING IN BENDING

The accuracy of the stiffness computed by the beam element is analyzed by a single leaf spring, shown in Fig. 5. The leaf spring is clamped at the base. The tip is displaced out of plane (i.e. in the y-direction), and the rotation about the x-axis and the z-axis are prescribed to be zero. The leaf spring is modelled by 5 serial connected non-prismatic beam elements. A model in ANSYS is used as a reference, where the leaf springs were modelled by about 15 000 solid-shell elements (SOLSH190), with three layers of elements in the thickness-direction. The length of the leaf spring is 100 mm and it is made out of steel with an elasticity modulus of 200 GPa and a Poisson ratio of 0.3. Four different designs are considered, one prismatic design and three designs where the width or thickness is varied linear from the base to the tip:

(P) Width: 40 mm, thickness: 0.5 mm
(W1) Width: from 60 to 40 mm, thickness: 0.5 mm
(W2) Width: from 80 to 40 mm, thickness: 0.5 mm
(T) Width: 40 mm, thickness: from 1.0 to 0.4 mm

Figure 6 shows the axial stiffness and in-plane stiffness during the tip-displacement. The axial stiffness is computed accurately by the beam elements. The results of the in-plane direction show some differences between the beam elements and ANSYS. The stiffness at zero displacement is correct for the prismatic case, but it deviates slightly for the two designs where de width is varied (i.e. W1 and W2). This is as the variation of the width is significant with respect to the length of the leaf spring which is known to result in a small error as shown by Boley [21]. The stiffness of the (T)-design at zero displacement is computed correct as the variation of the thickness is small compared to the length of the leaf spring. For all of the four designs, the in-plane stiffness becomes inaccurate after a significant displacement of the tip.

Table 1 shows the driving stiffness in undeformed configuration, showing a difference of about 5% between the non-prismatic beam element and ANSYS. The driving stiffness varies only a few percent during the tip-displacement and it is therefore modelled sufficiently accurate by the non-prismatic beam elements for the full range of motion.

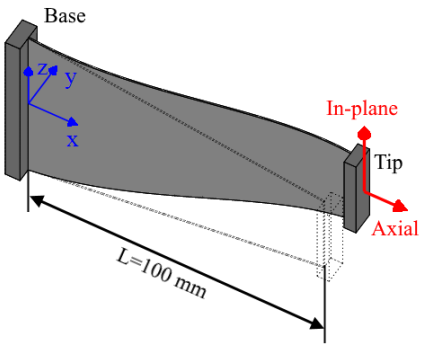

FIGURE 5: LEAF SPRING WITH OUT-OF-PLANE DIAPLACEMENT OF THE TIP

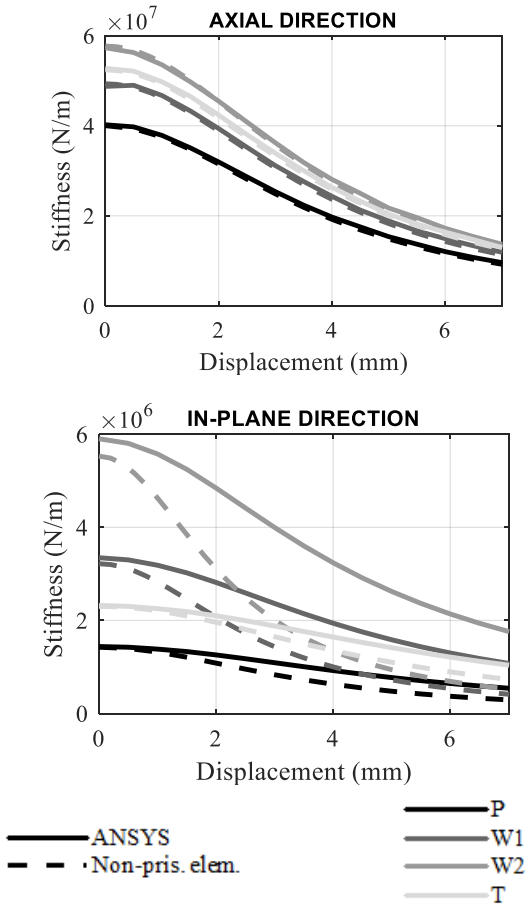

FIGURE 6: SUPPORT STIFFNESS OF THE LEAF SPRING DURING OUT-OF-PLANE DISPLACEMENT

TABLE 1: DRIVING STIFFNESS OF THE LEAF SPRING IN UNDEFORMED CONFIGURATION

	P	W1	W2	T
Non-prismatic element (N/mm)	1.00	1.24	1.45	2.43
ANSYS (N/mm)	1.05	1.32	1.55	2.57
Error (%)	4.6	6.3	5.9	5.4

4. OPTIMIZATION OF A PARALLEL FLEXURE GUIDANCE

To study the value of non-prismatic leaf springs compared to prismatic leaf springs, a parallel flexure guidance is optimized for support stiffness. Figure 7 shows the dimensions of the mechanism. The depth of the mechanism is 0.05 m and the elasticity of the flexures is 200 GPa with a Poisson ratio of 0.3. The mechanism should be able to move 0.02 m, without exceeding the stress limit of 600 MPa. The maximum stress in the material is computed based on the method explained in [27]. Four different design cases are considered for the shape of the leaf springs:

(P) prismatic leaf springs
(R) prismatic reinforced leaf springs, where the reinforced part is assumed to be infinite stiff and has length $0.1 \cdot d_{reinf}$.
(LR) reinforced leaf springs of which the thickness of the slender parts varies linearly over the length, determined by thickness t_1 (at the base) and t_3 (just before the reinforced part).
(QR) reinforced leaf springs of which the thickness of the slender parts varies quadratic over the length, determined by thickness t_1, t_3 and t_2 (at the center of the slender part).

Table 2 shows the optimized results for three different directions in which the support stiffness is optimized: in the y-direction, in the z-direction and the rotation around the x-axis, all evaluated in the initial center of compliance (the position of the frame in Fig. 7). The optimized designs for rotational support stiffness around the y-axis and z-axis are similar to the designs of the translational support stiffness in the z-direction and y-direction respectively and are therefore not shown in Table 2. The results indicate that the support stiffness can be increased by a factor of 1.4 till 1.9 by using reinforced non-prismatic leaf springs instead of reinforced prismatic leaf springs. Using a quadratic thickness variation only marginally increases the support stiffness with respect to a linear thickness variation.

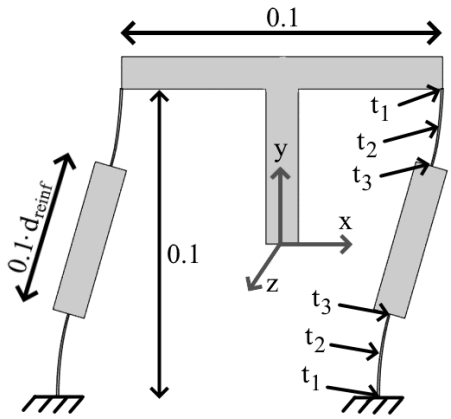

FIGURE 7: DIMENSIONS OF THE PARALLEL FLEXURE GUIDANCE. THE FRAME IS ATTACHED TO THE POINT WHERE THE STIFFNESS IS EVALUATED

TABLE 2: OPTIMIZED SUPPORT STIFFNESS AND CORRESPONDING DESIGN PARAMETERS FOR OPTIMIZED SUPPORT STIFFNESS IN THREE DIRECTIONS.

Case dir. K	De-sign	K_{opt} [1] Abso-lute	F.P.	Design parameters t_1 (mm)	d_{reinf}	t_3 (mm)	t_2 (mm)
y	P	3.2		0.50			
	R	9.7	3.03	0.30	0.73		
	LR	12.8	4.01	0.35	0.75	0.30	
	QR	12.9	4.01	0.34	0.75	0.30	0.32
z	P	0.27		0.50			
	R	0.27	0.99	0.50	0.00		
	LR	0.48	1.81	0.89	0.11	0.41	
	QR	0.51	1.89	0.92	0.14	0.39	0.69
θ_x	P	0.50		0.50			
	R	0.91	1.83	0.41	0.55		
	LR	1.63	3.27	0.65	0.49	0.46	
	QR	1.68	3.38	0.67	0.48	0.46	0.57

[1] The support stiffness is given as an absolute value in 10^6 N/m for the translational cases and in 10^3 Nm for the rotational cases. The second value (F.P.) is the support stiffness as a factor of the support stiffness of the prismatic case.

The designs are validated in ANSYS, where the flexures were modelled by about 15 000 solid-shell elements (SOLSH190) in total, with three layers of elements in the thickness direction. Table 3 shows the stiffness in the rotational stiffness around the x-axis computed in the undeformed configuration with the non-prismatic element and with ANSYS. The results indicates that the non-prismatic element results in an error of about 10% for both the prismatic design and only about 1% for the (non-prismatic) reinforced designs.

Figure 8 shows the stress distribution for design case (R) and design case (QR), indicating that the stress distribution over the length of the beam becomes almost constant for the QR-case. This was also observed for all the other non-prismatic designs. Table 3 shows the maximum stress computed by ANSYS, which is considerable higher than the maximum stress of 600 MPa computed by the non-prismatic beam elements. This is due to the fact that the beam element does not account for the anticlastic curvature effects as can be observed in Fig. 8: the QR-case in this figure shows that the stress is about 600 MPa over the whole area of the leaf springs except from the sides.

Figure 9 shows support stiffness, modelled with and without the second order expression for axial deformation as derived in Section 2.3. The stiffness result of the beam elements with the nonlinear axial deformation converge significantly faster to the accuracy that is reached by 8 serial connected elements. The computation time that is required for both elements is about the same. It is therefore useful to include the second order expression for axial deformation. The computation time to solve the total

TABLE 3: SUPPORT STIFFNESS IN UNDEFORMED CONFIGURATION AND STRESS RESULTS, FOR THE FOUR DESIGNS THAT ARE OPTIMIZED FOR STIFFNESS AROUND THE X-AXIS.

	P	R	LR	QR
K_{ox} – non-prismatic element (kNm)	20.8	38.2	44.9	44.7
K_{ox} – ANSYS (kNm)	20.6	38.5	45.2	45.3
K_{ox} – error (%)	0.80	0.70	0.69	1.3
Stress ANSYS	647	639	715	708

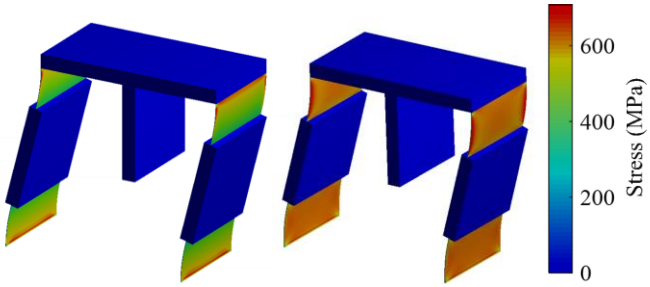

FIGURE 8: STRESS DISTRIBUTION OF THE OPTIMIZED SUPPORT STIFFNESS IN THE Y-DIRECTION FOR THE R-CASE (LEFT) AND THE QR-CASE (RIGHT)

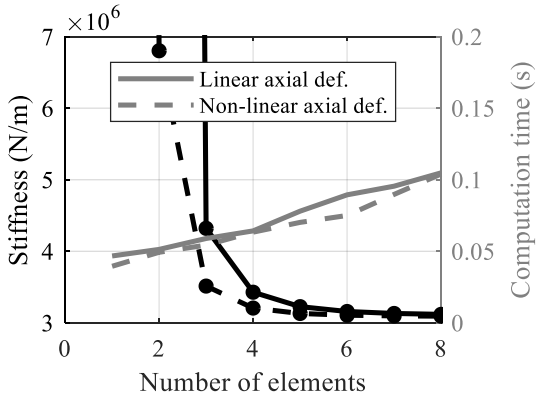

FIGURE 9: SUPPORT STIFFNESS IN Y-DIRECTION AND COMPUTATION TIME OF THE PRISMATIC DESIGN

displacement by ANSYS was 209 seconds for the model with 15 000 elements, and 32 seconds for a model with 4 000 elements (which gives an error of about 3% in the stress results). The model with the non-prismatic beam-elements is therefore significantly more efficient to evaluate.

5. OPTIMIZATION OF A FOLDED LEAF SPRING BASED SPHERICAL JOINT

Naves et all [28] proposed multiple configurations for a folded leaf spring based spherical flexure joint. In this section it is analyzed for two of these configurations to what extend non-prismatic instead of prismatic leaf springs can improve the performance:

(FL) The single folded leaf spring based spherical joint, consisting of 3 folded leaf springs, this is the most simple design in [28] and is shown in Fig. 10.

(SFL) The serial stacked folded leaf spring based spherical joint, consisting of two (FL)-joints. This was the best performing design in [28] and it is shown in Fig. 11.

Naves et all [28] optimized the joints for the support stiffness in the z-direction, when considering a range of motion of 30° tip-tilt angle (any rotation angle perpendicular to the z-axis). The maximum allowable stress in the material due to deformation is 600 MPa, the elasticity of the material is 200 GPa and the Poisson ratio is 0.3. The build space for the mechanism is limited to a cylinder aligned with the z-axis with a radius of 75 mm. The algorithm presented in [29] was used to detect collision of the leaf springs. Five design parameters were used, which are shown in Fig. 10. In this paper, the effect of using non-prismatic leaf springs is considered, using the same conditions as Naves, by considering 4 different design for each of the two mentioned configurations:

(P) Prismatic leaf springs (so exactly the same model as in [28])

(W) The thickness of the leaf springs is kept constant, while the width was varied quadratically. The width is determined by the width at the base (w_1), the width at the center (w_2) and the width at the fold (w_3)

(T) A constant width and a quadratically varying thickness, which is determined by t_1, t_2 and t_3, defined at the same positions as in case (W).

(WT) The width and the thickness are both varied quadratically.

Table 4 shows the optimized results, indicating that using non-prismatic instead of prismatic leaf springs increases the support stiffness up to a factor of 1.7. The support stiffness computed by the non-prismatic beam element is validated by ANSYS. Table 5 shows the support stiffness in the undeformed configuration for each of the four optimized designs of the SFL-configuration. It shows good results for the P-design and the T-design. However the stiffness computed with the non-prismatic beam element results in a small error if the width is varied, i.e. the W-design and the WT-design. This is understandable as the variation in the width is significant with respect to the length of the leaf-springs.

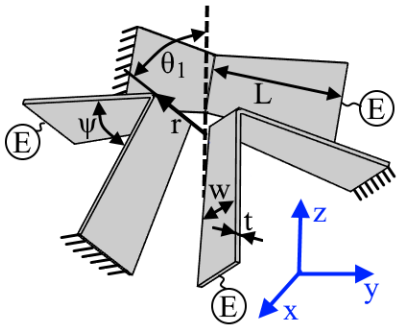

FIGURE 10: PARAMETERIZATION OF THE (FL)-JOINT. "E" REPRESENTS THE CONNECTIONS WITH THE END-EFFECTOR.

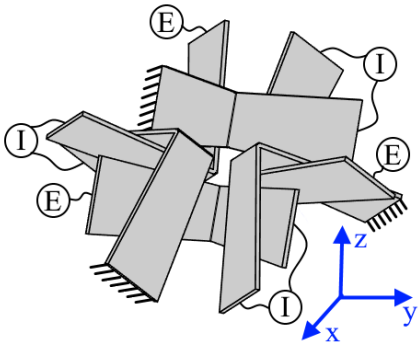

FIGURE 11: (SFL)-JOINT. "E" REPRESENTS THE CONNECTIONS WITH THE END-EFFECTOR, "I" THE CONNECTIONS WITH A RIGID INTERMEDIATE STAGE.

TABLE 4: OPTIMIZATION RESULTS OF THE FOLDED LEAF SPRING BASED SPHERICAL JOINT.

Case		K_{opt} [1]		Design parameters					
Con-fig.	De-sign	Abs.	F.P.	L (mm)	r (mm)	ψ (°)	θ_1 (°)	w [2] (mm)	t [2] (mm)
FL	P	182		71.0	28.5	85	43	27.5	0.64
	W	202	1.11	68.2	29.7	86	40	33.6 30.4 28.7	0.61
	T	205	1.13	68.6	31.8	87	42	30.9	0.65 0.61 0.59
	WT	219	1.20	68.9	28.2	86	40	31.7 35.2 26.4	0.66 0.59 0.67
SFL	P	923		64.8	37.8	102	40	35.0	0.98
	W	1595	1.73	61.6	36.2	93	36	49.3 37.9 33.2	1.03
	T	1488	1.61	61.9	43.1	98	39	41.3	1.25 0.97 0.88
	WT	1604	1.74	61.8	37.1	96	34	49.0 42.7 33.9	1.11 0.97 1.02

[1] The support stiffness is given as an absolute value in N/mm. The second value (F.P.) is the support stiffness as a factor of the support stiffness of the prismatic case.

[2] In the cases for a varying with or thickness, the values w_1, w_2, w_3 or t_1, t_2, t_3 are given respectively

TABLE 5: STIFFNESS OF THE SFL-JOINT IN Z-DIRECTION IN UNDEFORMED CONFIGURATION

	P	W	T	WT
Non-prismatic element (N/mm)	1 844	3 973	3 577	4 824
ANSYS (N/mm)	1 838	4 191	3 563	5 013
Error (%)	0.3	5.2	0.4	3.8

6. CONCLUSION

A non-prismatic beam element for the optimization of compliant mechanisms with non-prismatic leaf springs has been derived. The element allows for very efficient and relatively accurate analysis of compliant mechanisms. The element shows an error up to 10% for stress results and for stiffness in undeformed configurations, which is accurate enough for optimization purposes. The element is used in design optimizations to increase support stiffness. It is shown that the support stiffness of flexure joints can be increased, keeping the range of motion constant, by using non-prismatic instead of prismatic leaf springs. The support stiffness of a parallel flexure guidance increased up to a factor of 1.9 and that of a folded leaf-spring based spherical joint up to a factor of 1.7.

ACKNOWLEDGEMENTS

This work is part of the research programme HTSM 2017 with project number 16210, which is partly financed by the Netherlands Organisation for Scientific Research (NWO).

REFERENCES

1. Howell, L.L., "Compliant mechanisms. 2001: John Wiley & Sons.
2. Richard, M. and Clavel, R., "Concept of modular flexure-based mechanisms for ultra-high precision robot design," *Mechanical Sciences*, 2011. **2**(ARTICLE): p. 99-107.
3. Hao, G. and Kong, X., "A novel large-range XY compliant parallel manipulator with enhanced out-of-plane stiffness," *Journal of Mechanical Design*, 2012. **134**(6): p. 061009.
4. Wan, S. and Xu, Q., "Design and analysis of a new compliant XY micropositioning stage based on Roberts mechanism," *Mechanism and Machine Theory*, 2016. **95**: p. 125-139.
5. Zelenika, S., Munteanu, M.G., and De Bona, F., "Optimized flexural hinge shapes for microsystems and high-precision applications," *Mechanism and Machine Theory*, 2009. **44**(10): p. 1826-1839.
6. Wadikhaye, S.P., Yong, Y.K., and Moheimani, S.R. "Nanopositioner design using tapered flexures: A parametric study," in *2013 IEEE/ASME International Conference on Advanced Intelligent Mechatronics*. 2013. IEEE.
7. Tschiersky, M., Hekman, E.E., Brouwer, D.M., and Herder, J.L., "Gravity Balancing Flexure Springs for an Assistive Elbow Orthosis," *IEEE Transactions on Medical Robotics and Bionics*, 2019. **1**(3): p. 177-188.
8. Wiersma, D., Boer, S., Aarts, R.G., and Brouwer, D.M., "Design and performance optimization of large stroke spatial flexures," *Journal of computational and nonlinear dynamics*, 2014. **9**(1): p. 011016.
9. Naves, M., Brouwer, D.M., and Aarts, R.G., "Building Block-Based Spatial Topology Synthesis Method for Large-Stroke Flexure Hinges," *Journal of mechanisms and robotics*, 2017. **9**(4): p. 041006.
10. Jonker, J. and Meijaard, J., "SPACAR—Computer program for dynamic analysis of flexible spatial mechanisms and manipulators," in *Multibody systems handbook*. 1990, Springer. p. 123-143.
11. Jonker, J.B. and Meijaard, J.P., "A geometrically non-linear formulation of a three-dimensional beam element for solving large deflection multibody system problems," *International journal of non-linear mechanics*, 2013. **53**: p. 63-74.
12. Eisenberger, M. and Reich, Y., "Static, vibration and stability analysis of non-uniform beams," *Computers & structures*, 1989. **31**(4): p. 567-573.
13. Lee, S.Y., Ke, H.Y., and Kuo, Y.H., "Exact static deflection of a non-uniform Bernoulli-Euler beam with general elastic end restraints," *Computers & structures*, 1990. **36**(1): p. 91-97.
14. Friedman, Z. and Kosmatka, J., "Exact stiffness matrix of a nonuniform beam—II. Bending of a timoshenko beam," *Computers & structures*, 1993. **49**(3): p. 545-555.
15. Romano, F., "Deflections of Timoshenko beam with varying cross-section," *International journal of mechanical sciences*, 1996. **38**(8-9): p. 1017-1035.
16. Attarnejad, R., Shahba, A., and Semnani, S.J., "Analysis of non-prismatic Timoshenko beams using basic displacement functions," *Advances in Structural Engineering*, 2011. **14**(2): p. 319-332.
17. Cleghorn, W. and Tabarrok, B., "Finite element formulation of a tapered Timoshenko beam for free lateral vibration analysis," *Journal of Sound and Vibration*, 1992. **152**(3): p. 461-470.
18. Attarnejad, R., Semnani, S.J., and Shahba, A., "Basic displacement functions for free vibration analysis of non-prismatic Timoshenko beams," *Finite Elements in Analysis and Design*, 2010. **46**(10): p. 916-929.
19. Rao, S.S. and Gupta, R., "Finite element vibration analysis of rotating Timoshenko beams," *Journal of Sound and Vibration*, 2001. **242**(1): p. 103-124.
20. Awtar, S. and Sen, S., "A generalized constraint model for two-dimensional beam flexures: nonlinear load-displacement formulation," *Journal of Mechanical Design*, 2010. **132**(8): p. 081008.
21. Boley, B.A., "On the accuracy of the Bernoulli-Euler theory for beams of variable section," *Journal of applied mechanics*, 1963. **30**(3): p. 373-378.
22. Hodges, D., Ho, J., and Yu, W., "The effect of taper on section constants for in-plane deformation of an isotropic strip," *Journal of Mechanics of Materials and Structures*, 2008. **3**(3): p. 425-440.

23. Auricchio, F., Balduzzi, G., and Lovadina, C., "The dimensional reduction approach for 2D non-prismatic beam modelling: A solution based on Hellinger–Reissner principle," *International Journal of Solids and Structures*, 2015. **63**: p. 264-276.
24. Balduzzi, G., Aminbaghai, M., Sacco, E., Füssl, J., Eberhardsteiner, J., and Auricchio, F., "Non-prismatic beams: a simple and effective Timoshenko-like model," *International Journal of Solids and Structures*, 2016. **90**: p. 236-250.
25. Cowper, G., "The shear coefficient in Timoshenko's beam theory," *Journal of applied mechanics*, 1966. **33**(2): p. 335-340.
26. Besseling, J., "Non-linear theory for elastic beams and rods and its finite element representation," *Computer Methods in Applied Mechanics and Engineering*, 1982. **31**(2): p. 205-220.
27. Boer, S.E., Aarts, R., Brouwer, D.M., and Jonker, J.B. "Multibody modelling and optimization of a curved hinge flexure," in *The 1st joint international conference on multibody system dynamics, Lappeenranta*. 2010.
28. Naves, M., Aarts, R., and Brouwer, D., "Large stroke high off-axis stiffness three degree of freedom spherical flexure joint," *Precision engineering*, 2019. **56**: p. 422-431.
29. Naves, M., Aarts, R., and Brouwer, D.M., "Efficient collision detection method for flexure mechanisms comprising deflected leafsprings," *Journal of mechanisms and robotics*, 2018. **10**(6): p. 061012.